AIAA 2002–3158

Adaptive Identification and Control of Flow-Induced Cavity Oscillations

M. A. Kegerise
NASA Langley Research Center, Hampton, VA 23681

L. N. Cattafesta and C. Ha
University of Florida, Gainesville, FL 32611

1st AIAA Flow Control Conference
June 24–27, 2002/St. Louis, MO

Adaptive Identification and Control of Flow-Induced Cavity Oscillations

M. A. Kegerise*
NASA Langley Research Center, Hampton, VA 23681
L. N. Cattafesta† and C. Ha‡
University of Florida, Gainesville, FL 32611

Progress towards an adaptive self-tuning regulator (STR) for the cavity tone problem is discussed in this paper. Adaptive system identification algorithms were applied to an experimental cavity-flow tested as a prerequisite to control. In addition, a simple digital controller and a piezoelectric bimorph actuator were used to demonstrate multiple tone suppression. The control tests at Mach numbers of 0.275, 0.40, and 0.60 indicated $\approx 7dB$ tone reductions at multiple frequencies. Several different adaptive system identification algorithms were applied at a single freestream Mach number of 0.275. Adaptive finite-impulse response (FIR) filters of orders up to $N = 100$ were found to be unsuitable for modeling the cavity flow dynamics. Adaptive infinite-impulse response (IIR) filters of comparable order better captured the system dynamics. Two recursive algorithms, the least-mean square (LMS) and the recursive-least square (RLS), were utilized to update the adaptive filter coefficients. Given the sample-time requirements imposed by the cavity flow dynamics, the computational simplicity of the least mean squares (LMS) algorithm is advantageous for real-time control.

Introduction

THE flow over a cavity is characterized by a complex feedback process that leads to self-sustaining oscillations at a discrete set of frequencies. Often, these multiple "Rossiter modes" experience significant non-linear interactions and mode switching.[1,2] Cavity flows are of practical significance to aircraft with weapons bays. Here, the large sound pressure levels associated with the flow oscillations (> 170 dB) can be damaging to stores within the bay and can influence the trajectory of released stores. Cavity flows are also of interest as an active-control testbed. The problem is low-dimensional in the sense that only a few discrete modes are to be controlled, and only a small number of actuators and sensors are needed. This is in contrast to more complicated active control problems, such as turbulent boundary layer drag reduction, where the physics is infinitely dimensional and large numbers of distributed sensors and actuators are necessary.

Previous studies have considered the active control of cavity oscillations. Williams *et al.*,[2,3] employed a simple analog feedback controller to demonstrate multiple tone suppression at subsonic Mach numbers. Controller parameters were tuned manually to optimize suppression. While manual tuning of control parameters is not of practical interest, the experiments demonstrated the potential for feedback control. The controller also provides for quick evaluation of different actuator concepts. Cabell *et al.*[4] used discrete-time, linear quadratic control design methods for feedback control of cavity tones. The controller was successful in reducing the levels of multiple cavity tones at Mach numbers ranging from 0.275 to 0.45. Control performance was limited by excitation of sidebands of cavity tones, and the creation of new tones in the spectrum. These phenomena have recently been analyzed by Rowley *et al.*[5] and can, in part, be attributed to convective time delays between the actuator input and the output sensors (typically cavity-wall pressures). A linear quadratic regulator was also used by Cattafesta *et al.*[6] for single mode resonance at low Mach numbers (< 0.15).

An important limitation of standard feedback control schemes is that they cannot compensate for changes in system dynamics. The system dynamics of cavity flows change as flow conditions are altered. There is also the question of whether system dynamics change under the application of control. Either case necessitates re-identification of the system dynamics for control design. Adaptive controllers offer promise to overcome the limitations imposed by standard methods. They can adapt to changing flow conditions, can provide automatic tuning of controller parameters for optimal performance, and have built in system monitoring and fault tolerance. Adaptive controllers have already been applied to the cavity problem. Williams *et al.*[7] employed an adaptive feed-

*Research Scientist. Flow Physics and Control Branch. Member AIAA.

†Assistant Professor. Senior Member AIAA.

‡Graduate Research Assistant. Student Member AIAA

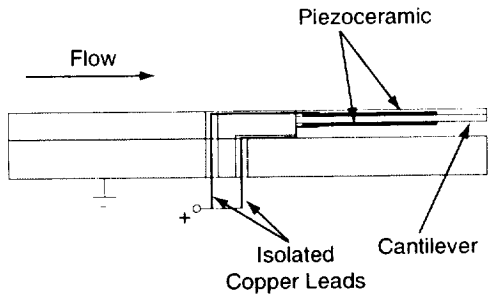

Fig. 3 Schematic of piezoelectric bimorph actuator assembly.

Piezoelectric Bimorph Actuator

In cavity control, the objective of the actuator is to produce a disturbance equal and opposite to the natural one produced by acoustic feedback. To meet this objective, any actuator for cavity control must meet a certain set of requirements. The actuator must have a bandwidth as large as the maximum Rossiter frequency of interest (~ 1 kHz in the present case). The requirements for the actuator amplitude response are not known *a priori* because the disturbance levels at the shear-layer origin are not typically known. However, it is desired to have a response that can produce a broadband disturbance rather than a single tone. Finally, the actuator should be situated such that it introduces disturbances at the cavity leading edge where the flow is most receptive. A flap-type actuator provides a good balance between these requirements and was thus chosen for the present work.

The flap-type actuator is a piezoelectric bimorph cantilever beam. Figure 2 shows the actuator installation in the wind-tunnel model. The tip of the beam is coincident with the cavity leading edge. The actuator was designed with a structural dynamics model and an optimization scheme. Given a desired natural frequency, the design parameters are calculated such that the target frequency is achieved *and* tip displacement is maximized. The target frequency for the present actuator was 1500 Hz and the calculated DC gain was 0.25 $\mu m/V$. Further details of the design methodology are beyond the scope of this work and the interested reader can refer to the papers by Cattafesta *et al.*[10,11]

Table 1 Design parameters of piezoelectric bimorph actuator.

Quantity	Value
Shim length, mm	25.4
Piezo length, mm	17.8
Shim thickness, mm	0.89
Piezo thickness, mm	0.38
Shim width, mm	48.0
Piezo width, mm	48.0

A schematic of the bimorph actuator assembly is shown in Figure 3 and a listing of the design parameters is provided in Table 1. The cantilever beam portion of the actuator was machined from aluminum. The piezoceramic wafers (PZT 5H) were bonded to the cantilever beam with a non-conductive epoxy adhesive. The actuator structure and cantilever beam were electrically grounded for safety reasons. High voltage was applied to the electrodes of the piezoceramics with isolated copper flat leads in a parallel configuration. A fairing layer of Kapton was placed on the top surface of the cantilever structure to provide a smooth surface for the incoming boundary layer.

A fiber-optic sensor was embedded in the front wall of the cavity model to provide an *in situ* measurement of the actuator displacement. Due to physical constraints imposed by the cavity model design, it was not possible to place the sensor at the actuator tip. Instead, the actuator was located 4 mm from the tip and offset 9 mm from the actuator centerline.

The *in situ* measurement of displacement is important for several reasons. The actuator frequency response can be measured in wind-on and wind-off conditions. This measurement will answer the question of whether flow over the actuator surface changes the dynamic response. More importantly, the displacement levels necessary for suppression of cavity tones can be quantified. This information can then be fed back into the design stage for future actuator generations.

Data Acquisition and Processing

The data acquisition and processing systems are described in this section. Depending on the purpose of the experiments, three different data systems were used.

To measure the bimorph transfer function, the actuator was excited with a chirp signal produced by a function generator. The frequency of the chirp signal was swept from 10 Hz to 2 kHz in 200 $msec$. The chirp signal was input to a high-voltage amplifier with a nominal gain of 100. The output of the amplifier was applied to the bimorph actuator. The signals from the function generator (input) and the displacement sensor (output) were bandpass filtered from 1 Hz to 4 kHz and sampled at 10.24 kHz with a 16-bit A/D. The data were subsequently processed to produce estimates of the transfer function.

For the digital control experiments, the front-wall pressure (error signal) was amplified to ± 10 V and bandpass filtered from 1 Hz to 16 kHz. This signal was sampled at 40 kHz with a 16-bit A/D card of a dSPACE digital control system. The real-time controller calculated the control signal once per time step using a single-processor dSPACE DS1005 card that utilizes a PowerPC7509 processor running at 480 MHz. The digital control signal was converted to the analog domain with a 14-bit D/A card. The control signal was routed to a reconstruction filter ($f_{cut} = 16$ kHz) to smooth the zero-order hold signal from the D/A card.

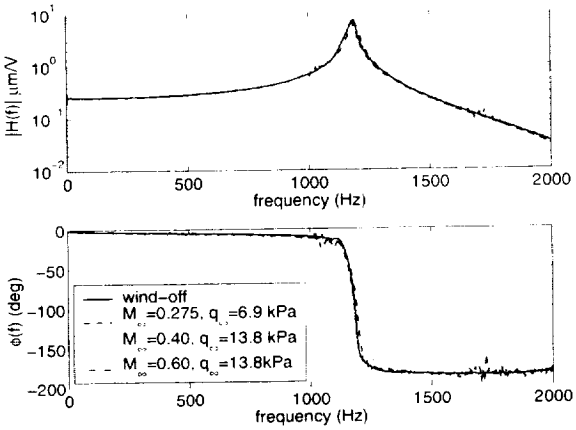

Fig. 6 Frequency response function of the piezoelectric bimorph actuator

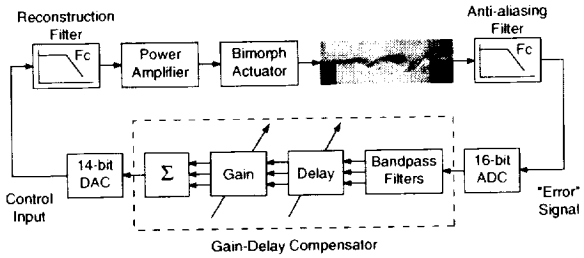

Fig. 7 Digital gain-delay feedback controller.

A schematic of the feedback controller is shown in Figure 7. The primary component of the controller consists of a gain-delay compensator that was programmed in SIMULINK and converted to compiled code that runs on the dSPACE DS1005 card. The sample time for the controller was 25 μsec. The compensator processes the "error" signal (front-floor pressure) as follows. The error signal is passed through a bank of digital bandpass filters (4th-order elliptic filters). Each filter is centered on a particular Rossiter mode. The signals from the digital filters are then passed through a delay of n samples and a gain a K. Note that these values are different for each Rossiter mode. Finally, the resulting signals are summed and output from the dSPACE system via the 14-bit D/A card. The parameters of the gain and delay blocks are tuned manually to minimize some performance measure. In the present case, the rear-wall pressure sensor was considered to be the performance measure and the compensator parameters were adjusted to minimize the tonal levels of each Rossiter mode lying within the actuator bandwidth. It should be noted that this type of controller is not new. Recently, Williams *et al.*[2,3] utilized this controller (in both the analog and digital domain) for cavity control studies. The gain-delay compensator was also used for feedback control of impinging-jet resonance[13] and vortex shedding from a cylinder in cross flow.[14]

Typical control results for three test conditions are shown in Figures 8, 9, and 10. The plots present

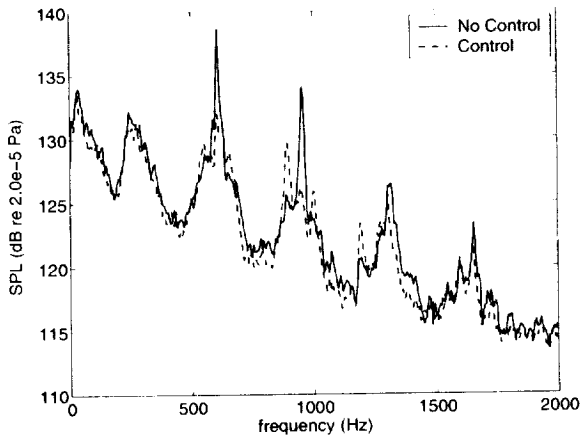

Fig. 8 Control performance at $M_\infty = 0.275$.

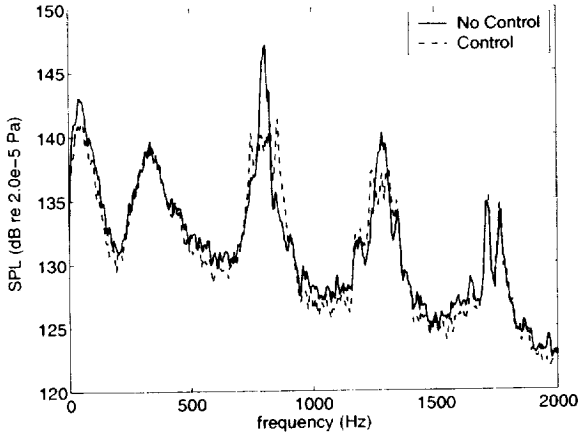

Fig. 9 Control performance at $M_\infty = 0.40$.

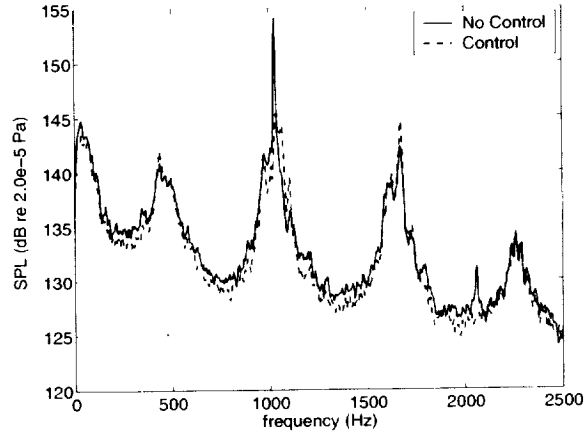

Fig. 10 Control performance at $M_\infty = 0.60$.

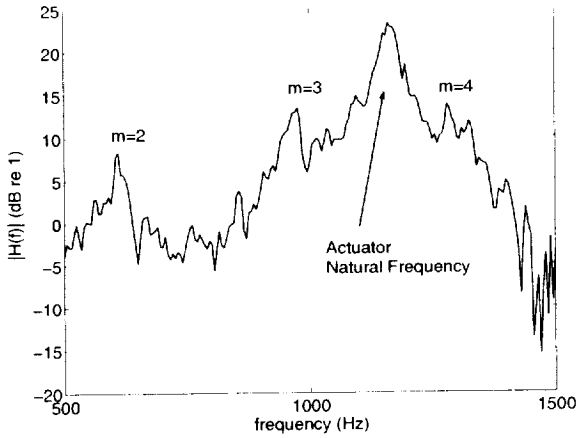

Fig. 12 Measured transfer function magnitude between actuator input and rear-wall pressure.

An important issue in adaptive control is that all computations must be completed within the sampling interval. The sampling interval is dictated by the frequency content of the process to be controlled. According to the Nyquist criterion, the sampling rate must be at least twice the highest frequency of interest. In the present case of cavity flow control, a sampling frequency of 5.12 kHz is desirable (sampling time of 195.3 μsec). The turnaround time, T_a, is defined as the time required to perform all the necessary calculations for a particular algorithm. Obviously, this must be smaller than the sample time, T_s. Further, the turnaround time associated with system identification should be somewhat less that the sample time to allow for the computations needed by the adaptive control scheme.

The system identification algorithms were applied to a single flow condition ($M_\infty = 0.275$). This flow condition is attractive because there are three Rossiter modes within the actuator bandwidth and therefore offers the greatest challenge to the identification algorithms. The actuator was driven with bandlimited (500-1500 Hz) colored noise (as described earlier) and the wall-pressure sensor signals were acquired. Prior to running the algorithms, input-output time series were recorded and the transfer function between them was calculated. This calculation was performed with standard FFT-based methods applied to 1024 point blocks, a Hanning window with 50% overlap, and 160 block averages. The result will be compared to the transfer functions identified by the adaptive algorithm in the following discussion. The transfer function magnitude between the input and output (rear-wall pressure) is shown in Figure 12. The figure is annotated to show the peaks associated with Rossiter modes $m = 2, 3, 4$. The large gain in the vicinity of 1200 Hz is due to the actuator dynamics. The magnitude of the transfer function outside of the 500-1500 Hz band is meaningless since there is no input.

Adaptive FIR Filter Results

Results for the FIR-LMS algorithm are shown in Figures 13a and 13b. The filter order for the data shown is $N = 100$. The turnaround time of this algorithm and filter order was 64 μsec. Time series of the system output (rear-wall pressure) and the adaptive filter output are shown in Figure 13a. The error between them, $d(n) - y(n)$, is also shown. As seen in the figure, the error between these two signals is significant.

The coefficients of the adaptive filter vary somewhat over time, and so the "instantaneous" transfer function varies with time. However, the coefficients vary about well defined mean values, suggesting some level of time invariance in the process. It is of interest then to consider whether the coefficients of the filter represent a transfer function that is, in an average sense, the measured transfer function of the system. To this end, the transfer function obtained from the filter coefficients at each time step was block averaged (in total, 2048 averages were used). The results are shown in Figure 13b. As observed in the figure, this average transfer function is not a good representation of the system dynamics.

Results for the FIR-RLS algorithm are shown in Figure 13c and 13d. The maximum filter order in this case was limited to $N = 20$, with a turnaround time of 136 μsec. It is clear that the computational requirements for the RLS algorithm are higher than for the LMS algorithm. This lower-order filter does a poor job of identifying the system dynamics.

Adaptive IIR Filter Results

Results for the adaptive IIR filters are shown in Figure 14. Adaptive IIR-LMS equation-error results are shown in Figure 14a and 14b. Here, the order of the moving-average coefficients was $M = 60$ and the order of the auto-regressive coefficients was $N = 100$. This filter does a good job of identifying the system dynamics in both the time and frequency domains. As seen in Figure 14b, the transfer function of the adaptive filter matches the measured transfer function in the vicinity of the Rossiter modes. The dynamics in the vicinity of the actuator natural frequency are, however, poorly matched. It is of interest to note that the turnaround time for this algorithm was 85 μsec. Thus, relatively high-order filters can be used while leaving computational resources for controller calculations.

The results for the adaptive IIR-LMS output-error algorithm are not shown. This is because the adaptive filter was not stable for any combination of filter parameters. Recall that the stability of IIR filters is not guaranteed. Further study is required to better understand the failure of this algorithm.

The IIR-RLS equation-error results are shown in Figure 14c and 14d. The maximum filter order that could be run in real-time was of 14th-order. The

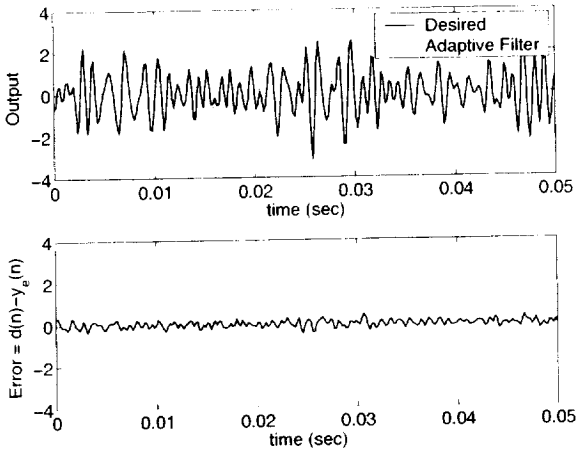

a) IIR LMS equation-error algorithm ($M = 60$, $N = 100$).

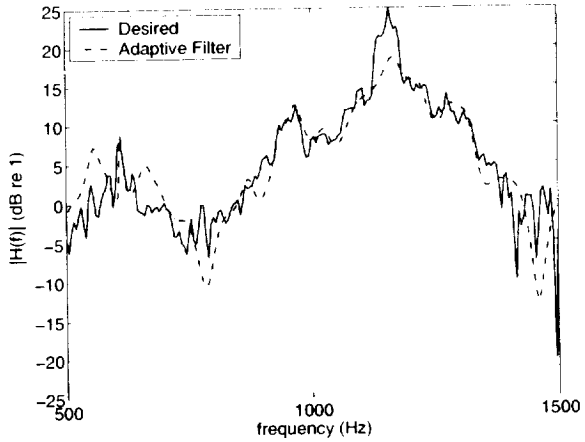

b) Measured and modeled transfer function magnitude from actuator to rear-wall pressure sensor (IIR LMS equation-error, $M = 60$, $N = 100$).

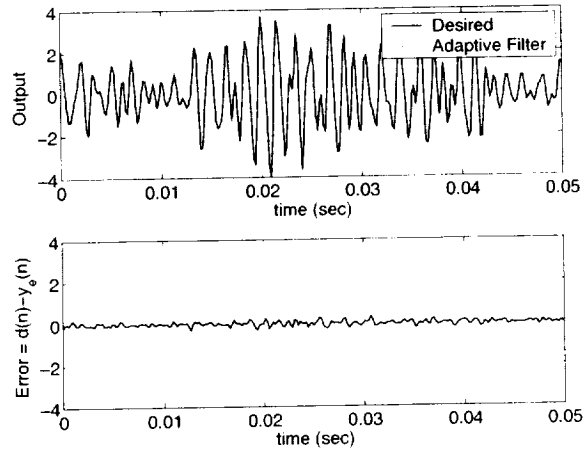

c) IIR RLS equation-error algorithm ($M = 14$, $N = 14$).

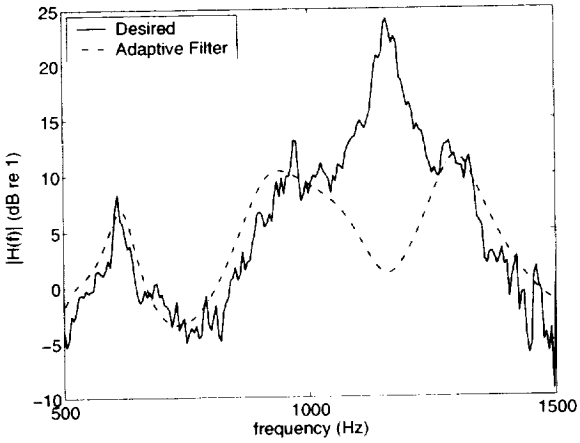

d) Measured and modeled transfer function magnitude from actuator to rear-wall pressure sensor (IIR RLS equation-error, $M = 14$, $N = 14$).

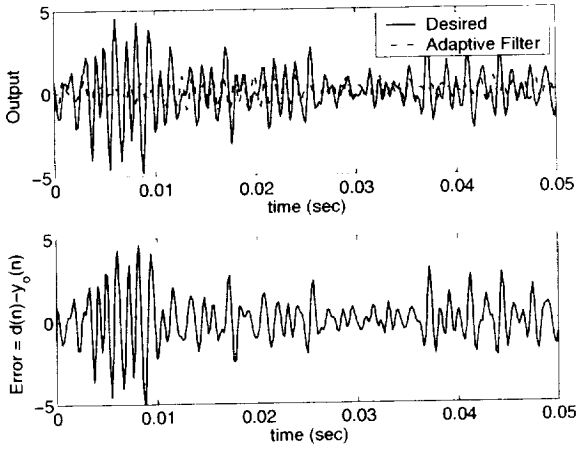

e) IIR RLS output-error algorithm ($M = 14$, $N = 14$).

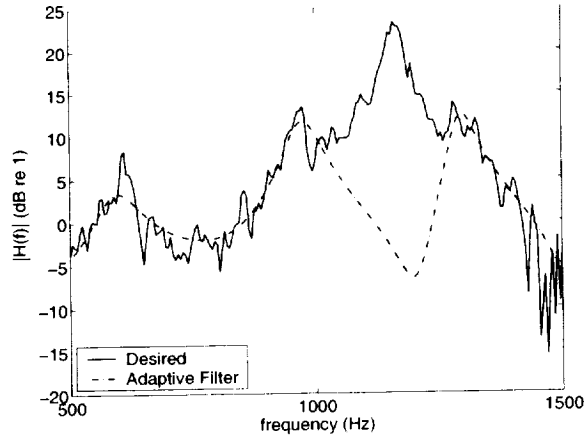

f) Measured and modeled transfer function magnitude from actuator to rear-wall pressure sensor (IIR RLS output-error, $M = 14$, $N = 14$).

Fig. 14 Comparison of adaptive IIR filters to measured response.